

CORMASS: A COMPACT AND EFFICIENT NIR SPECTROGRAPH FOR STUDYING LOW-MASS OBJECTS¹

J.C. WILSON², M.F. SKRUTSKIE³, M.R. COLONNO⁴, A.T. ENOS⁴, J.D. SMITH⁴, C.P. HENDERSON⁴, J.E. GIZIS⁵, D.G. MONET⁶ AND J.R. HOUCK⁴
PASP, accepted 30 Oct 2000

ABSTRACT

CorMASS (Cornell Massachusetts Slit Spectrograph) is a compact, low-resolution ($R \sim 300$), double-pass prism cross-dispersed near-infrared (NIR) spectrograph in operation on the Palomar Observatory 60-inch telescope. Its 2-dimensional spectral format provides simultaneous coverage from $\lambda \sim 0.75\mu\text{m}$ to $\lambda \sim 2.5\mu\text{m}$ ($zJHK$ bands). A remotely operated cold flip mirror permits its NICMOS3 detector to function as a K_s slit viewer to assist object placement into the $2'' \times 15''$ slit. CorMASS was primarily designed for the rapid spectral classification of low-mass stellar and sub-stellar objects identified by the Two-Micron All Sky Survey (2MASS). CorMASS' efficiency and resolution also make it a versatile instrument for the spectral observation and classification of many other types of bright objects ($K < 14$) including quasars, novae, and emission line objects.

Subject headings: infrared: stars — instrumentation: spectrographs — stars: low mass, brown dwarfs

1. INTRODUCTION

Recent successes by deep near-infrared (NIR) surveys such as the Two Micron All Sky Survey (2MASS; (Skrutskie et al. 1997)), the Deep Near-Infrared Survey (DENIS; (Epchtein 1997)), and the Sloan Digital Sky Survey (SDSS; (Gunn & Weinberg 1995)) in identifying very low-mass stellar and sub-stellar field candidates have made a tremendous impact upon the study of low-mass objects in the local stellar neighborhood. Spectroscopic follow-up of low-mass survey candidates has revealed objects with atmospheric features different from the TiO and VO features seen in the atmospheres of M-dwarfs. Two new classifications, L with $1300 \lesssim T_{\text{eff}} \lesssim 2000$ (Kirkpatrick et al. 2000a) and T with $T_{\text{eff}} \lesssim 1200 - 1300$ (Fegley & Lodders 1996; Burrows & Sharp 1999; Kirkpatrick et al. 2000a), have been proposed to account for the unique spectral characteristics of these objects at and below the bottom of the main sequence (Martín et al. 1997; Kirkpatrick et al. 1999). L-dwarf spectra are dominated by metallic hydrides and alkali atomic features as the oxides of M-dwarfs condense into solids at these cooler atmospheric temperatures. T-dwarfs show the distinctive CH_4 absorption features at $1.6\mu\text{m}$ and $2.2\mu\text{m}$. Gl 229B is the archetypical T-dwarf (Nakajima et al. 1995; Oppenheimer et al. 1998).

Motivated by the potential identification of a few 10^3 candidate L and T-dwarfs in the northern sky by 2MASS (Reid et al. 1999), we have built a spectrograph specifically for the efficient confirmation and classification of low-mass

object candidates. This paper describes the Cornell Massachusetts Slit Spectrograph (CorMASS) and presents a sample of spectral observations from its first runs on the Palomar 60-inch telescope.

CorMASS is a double-pass prism cross-dispersed NIR grating spectrograph. Simultaneous wavelength coverage spans from $\lambda \sim 0.75\mu\text{m}$ to the 256×256 HgCdTe NICMOS3 array cut-off at $\lambda \sim 2.5\mu\text{m}$ (the $zJHK$ photometric bands)⁷. This wavelength coverage is dispersed into 6 orders on the array. A spectral resolution of $R \equiv \lambda/\Delta\lambda \sim 300$ maximizes signal from relatively faint objects, while keeping resolution high enough to identify features of the target between blended airglow lines, including in H-band. An externally driven cold flip mirror permits the reflective slit to be imaged in K_s on the NICMOS3 array using a complementary optical train.⁸ The slit viewer's $35''$ field-of-view (FOV) enables rapid object identification and accurate placement of science targets into the slit for spectroscopy. The compact instrument optical and mechanical design occupies an LN_2 cooled volume of $14.5'' \times 6.5'' \times 6''$ inside the Dewar.

After presenting our scientific requirements for the instrument in §2, the optical design is discussed in §3. The mechanical design is discussed in §4. Electronics and Data Acquisition are covered in §5. In §6 we discuss performance, and in §7 data reduction is discussed and sample spectra are presented.

¹ Observations made at the Palomar Observatory were made as part of a continuing collaboration between the California Institute of Technology and Cornell University. The 60-inch telescope at Palomar Mountain is jointly owned by the California Institute of Technology and the Carnegie Institution of Washington.

² Space Sciences Building, Cornell University, Ithaca, NY 14853; jcw14@cornell.edu

³ Department of Astronomy, University of Massachusetts, Amherst, MA 01003

⁴ Space Sciences Building, Cornell University, Ithaca, NY 14853

⁵ Infrared Processing and Analysis Center, M/S 100-22, California Institute of Technology, Pasadena, CA 91125

⁶ U.S. Naval Observatory, P.O. Box 1149, Flagstaff, AZ 86002

⁷ z is a SDSS photometric band with $\lambda_c = 0.91\mu\text{m}$ and $\Delta\lambda = 0.12\mu\text{m}$. The long wave cut-off is determined by CCD sensitivity (Fukugita et al. 1996).

⁸ K_s is a passband created for the 2MASS survey by one of us (M. Skrutskie). This band is shortened and shifted blue-ward compared to the conventional K -band to reduce in-band thermal emission (Persson et al. 1998).

2. SCIENCE REQUIREMENTS

We desired an instrument that could rapidly provide identifying spectra for candidate low-mass objects identified by 2MASS to within 1-2 spectral sub-classes. To accomplish this the instrument requires access to telltale L and T-dwarf identifying features in the red-optical such as CrH and FeH at $0.86\mu\text{m}$, H_2O at $0.94\mu\text{m}$, the FeH feature at $0.99\mu\text{m}$, as well as CH_4 features at $1.6\mu\text{m}$ and $2.2\mu\text{m}$ (Kirkpatrick et al. 1999). Other features important to NIR classification include the K I resonance doublets at $1.17\mu\text{m}$ and $1.24\mu\text{m}$, broad H_2O absorption features, and the CO bandhead at $2.29\mu\text{m}$.

The instrument's resolution must be as low as possible to maximize signal from intrinsically faint low-mass objects, yet high enough to detect identifying features between blended airglow lines. Since the airglow lines are most plentiful and intense in H-band, we chose the lowest resolution that retained the ability to observe the $1.6\mu\text{m}$ methane absorption feature between blended airglow lines, thus preserving the ability to identify this telltale T-dwarf spectral feature for the faintest objects.

Observing efficiency was paramount if the instrument were to quickly identify large numbers of objects and select those that warranted higher resolution and S/N study on larger telescopes, especially given the large number of L-dwarfs expected to be found by surveys. This requirement favored a cross-dispersed spectrograph with its efficient 2-D spectral format.

A NIR slit viewing mode was deemed imperative for rapid field identification and for steering objects accurately into the slit. Most science targets for this spectrograph have extreme visible-IR colors, i.e. CorMASS science targets tend to be visibly faint but IR bright.

The choice of slit width was driven by the typical seeing at the Palomar 60-inch of $\theta_{\text{FWHM}} \sim 1''$. To achieve Nyquist sampling at $2 \times \theta_{\text{FWHM}}$, we chose a $2''$ slit and a plate scale of $1''/\text{pixel}$. We desired the slit length to be as long as possible to sample the sky for accurate subtraction ($20''$ if possible), but left the final length to be determined by the optical design constraints.

Lastly, we wanted the instrument to have first light within one year of commencing design due to the rapidly progressing field of low-mass objects. For cost and schedule reasons we decided to modify an existing IR Labs Dewar and use an existing NICMOS 3 array and array electronics.

3. OPTICAL DESIGN

3.1. Palomar 60-inch

The Palomar 60-inch telescope is an equatorial mounted $f/8.75$ Ritchey-Chrétien design (Bowen & Rule 1966). Table 1 includes the telescope prescription. CorMASS mounts directly to the instrument mounting plate at the Cassegrain focus, as shown in Figure 1. With the exception of the primary and secondary mirrors and the Dewar window all the optical elements are cooled to LN_2 temperature.

3.2. Design Constraints

CorMASS features a compact design that was constrained by the existing Dewar and the telescope focus position.

3.2.1. Dewar Modification

The CorMASS Dewar previously served as the 2MASS Prototype Camera Dewar and more recently for testing NICMOS 3 arrays for the 2MASS survey. The original Dewar is an Infrared Laboratories (Tucson, AZ) ND-2(8)MOD Dewar with a 4.5 liter LN_2 tank and double shielding. It has a usable cold instrument volume of $\phi 7.5$ inches $\times \sim 5$ inches. It was clear that a Dewar expansion was required to increase the cold volume available for the new spectrograph optics. Clearly the simplest Dewar modification would be a cylindrical extension of the Dewar walls and shields. Thus the new spectrograph was constrained to $\phi < 7.5$ inches, with the length a 'free parameter.'

3.2.2. Telescope Focus Position

The optimal telescope focus is only ~ 35 mm below the instrument mounting plate (Table 1). In addition, a permanently mounted offset guide camera and filter motor assembly on the telescope instrument mounting plate constrain the outer diameter of an instrument mounted flush to the plate to be $\lesssim 10$ inches.

These constraints on access made placement of a cold slit at the telescope focus difficult. The awkward focus position was good incentive to allow the beam to diverge past the telescope focus, enter the cryogenic Dewar, and then re-image the beam onto a slit. Such a scheme would provide straight-forward $f/\text{conversion}$ between the telescope focus and slit, as well as produce a well-defined cold pupil stop. But a re-imaging scheme would further lengthen the cylindrical axis of the instrument, thus increasing expense, flexure and the moment arm of the instrument mass that must be compensated with telescope balance.

We chose instead the more compact scheme of placing a cold slit at the telescope focus. This required a very tightly integrated mechanical design just inside the window: the Dewar top plate, CaF_2 window, two radiation shield tops, and slit occupy a span of ~ 35 mm measured along the optical axis. $f/\text{conversion}$ is accomplished as the beam diverges past the cold slit. The clearance between the instrument mounting plate and the telescope fork is 38 inches. The final design length of CorMASS measures 27.7 inches. Figures 2 & 3 show the design of CorMASS.

3.3. Spectrograph Optics

3.3.1. Prescription

Ray tracing, optimization, and tolerancing for the CorMASS optical design was accomplished with the optical design software ZEMAX Version 6.0 (Focussoft, Tucson, AZ). The optical layout of CorMASS is shown in Figure 4. All five lenses are spherical and one is from stock while the remaining four are custom manufactured using in-house test-plates by Janos Technology, Inc. (Townshend, VT).

The main dispersing element is a coarse 40 lines mm^{-1} grating, blazed at $4.8\mu\text{m}$. A prism made from the Schott Dense Flint SF-10 is used in double-pass for cross-dispersion. Table 1 lists the spectrograph prescription.

After passing through the CaF_2 Dewar window, the converging telescope beam reaches a focus at the slit. A

wire electrical discharge machine (EDM) was used to cut a $185\mu\text{m} \times 951\mu\text{m}$ slit into the center of a .008" thick stainless steel (SS304) disk that had been hand polished with $1\mu\text{m}$ diamond paper. Ron Witherspoon Inc. (Campbell, CA) manufactured the slit. The disk is rotated 45 deg about the axis of the slit length so that incoming light not transmitted through the slit is reflected into the slit viewing train. The slit width is oversized by $\sqrt{2}$ to compensate for the disk rotation.

Past the slit the beam is converted from $f/8.75$ to $\sim f/14$ by an Infrasil 301-CaF₂ air-spaced doublet⁹ and is collimated by a gold-coated, diamond-turned, aluminum alloy (6061-T6) off-axis paraboloid. The beam then passes through a cold Lyot Stop sized to the pupil diameter of 22.6 mm. After the stop the beam passes through the SF-10 prism for the first cross-dispersion pass. The prism has a 30 deg apex angle and is used at minimum deviation. It was fabricated by Kreischer Optics, Ltd. (McHenry, IL).

A prism was necessary as the cross-dispersing element because the desired wavelength coverage exceeded a factor of 2. A double-pass prism design was adopted because it could be implemented in combination with the grating to produce a very compact optical package. When the dispersing elements were ordered in series [*prism pass 1 (cross dispersion) – grating reflection (primary dispersion) – prism pass 2 (cross dispersion)*] the optical path was neatly returned into the main '2-d' plane of the optical bench (Figures 2 - 4). Single-pass prism designs led to cubical mechanical packages that could not be simply inserted into the dewar.

In addition to SF-10 various other prism materials were considered, including AMTIR1 and ZnSe. Both have higher dispersion in the NIR than SF-10 but were rejected due to coating difficulty and expense. The use of a material easily coated was imperative for the reduction of Fresnel reflection losses at the four vacuum-prism interfaces encountered with a prism used in double-pass.¹⁰ The dispersion of SF-10 and the resulting order separation is discussed in §3.3.2.

The measured internal transmission of SF-10 (kindly provided by Dr. E. Oliva) and expected Anti-Reflection (AR) coating performance (Janos Technology, Inc.) are plotted in Figure 5. The transmission measurement was performed as described in Oliva & Gennari (1997) and includes theoretical Fresnel losses from two air-glass interfaces (dashed line) and internal transmission through one pass of a 21.7 mm uncoated sample (dotted line). This is very close to the median length of SF-10 traversed by the CorMASS beam in one pass (20.7 mm), so the plotted transmission, neglecting Fresnel losses, accurately reflects the expected internal transmission in our instrument. Shortward of $1.2\mu\text{m}$ the glass is nearly transparent. We assume absorption features longward of $1.4\mu\text{m}$ are due to water/OH in the glass. Combining the expected reflection losses through two air-glass interfaces after AR coating (long dashed line) with the internal transmission gives the total expected transmission through one prism pass for CorMASS (solid line). While the transmission losses

were unfortunate, they were accepted because the primary spectral features in K -band for L and T-dwarfs, the CO bandhead at $2.29\mu\text{m}$ and the $2.2\mu\text{m}$ CH₄ feature, resp., were deemed less important and redundant compared to the ζJH band features.

Following the first pass through the prism the beam is diffracted by the grating. Richardson Grating Labs (Rochester, NY) mounted an epoxy replica of a stock master grating onto an aluminum alloy (6061-T6) substrate provided by us. The gold coated grating, with 40 lines/mm groove density and blazed at 5.5° , is used with a turn-angle of 21.5° to match the angular beam deviation of the off-axis paraboloid for optical layout symmetry. The first order blaze wavelength (λ_B) is $4.71\mu\text{m}$. The detector images the 2nd through 9th orders, with coverage from $2.5\mu\text{m}$ to H α ($0.6563\mu\text{m}$). We designed the spectrograph to use orders 2-5 and were fortunate that orders 6-7 are in good optical focus as well. In practice only 2nd through 6th orders have useful throughput. (Spectrograph throughput is discussed in §6).

Inadvertently the shortward edge of order 2 and longward edge of order 3 are cutoff by the array edges, resulting in a gap in spectral coverage from $2.014 - 2.035\mu\text{m}$. Evidently the final spectrograph camera focal length is too long, likely due to errors in our assumed cryogenic indices of refraction.

Grating efficiency is well described by scalar theory if $\lambda/d < 0.2$ where d is the groove spacing ($25\mu\text{m}$ for CorMASS). Therefore, polarization effects are very small (Loewen et al. 1977). Theory also predicts $\gtrsim 50\%$ efficiency from $2/3\lambda_B$ to $1.8\lambda_B$ in first order. At higher orders this efficiency will be maintained because the grating is used even farther into the scalar domain as λ/d decreases (Loewen et al. 1977). A check of our chosen grating parameters in a commercial software program for grating efficiency analysis (PC Grate, Optometrics, Ayer, MA) yields estimated peak efficiencies of 90% for orders 2-5.

After diffraction by the grating, the beam passes through the prism for a second time. Lastly, the beam is focused onto the detector by an $f/5.5$ camera which delivers a final plate scale of $1''/\text{pixel}$ to the $40\mu\text{m}$ square NICMOS 3 pixels. The camera features three elements in a doublet-singlet format. Following a BaF₂-Infrasil air-spaced doublet, there is a space of ~ 5 inches before the converging beam passes through the final Infrasil lens and focuses on the detector. The final lens and detector are separated by ~ 1 inch.

The ratio of the telescope central obscuration diameter to primary diameter is $\epsilon = 0.3$. For a telescope with $\epsilon = 0.33$ the Encircled Energy fraction (EE) within the first Airy dark ring is 0.65 (Schroeder 1987). We used this EE benchmark to judge the image quality of the spectrograph design. Shortward of $2.2\mu\text{m}$ all wavelengths image $\text{EE} \geq 0.65$ within 1 pixel (Figure 6). This applies for the entire slit FOV ($2'' \times 15''$).

3.3.2. Order Format

⁹ Infrasil 301 is a water-free fused quartz made by Heraeus-Amersil Corp. (Duluth, GA).

¹⁰ We became aware of SF-10 during a search of stock prism vendors. Interestingly, the Schott 'SF' dense flint glasses have a partial dispersion similar to the alkaline-earth fluoride crystals (e.g. BaF₂, SrF₂, and CaF₂). This makes the SF glasses an appealing 'flint' to couple with the crystals to form achromatic NIR cameras (Oliva & Gennari 1997).

The SF-10 prism in CorMASS leads to an order format similar to that found when a first order grating is used as the cross-disperser¹¹; CorMASS' order separation increases with increasing wavelength (Figure 7), whereas prism cross-dispersers typically give larger order separation for decreasing wavelength. The CorMASS format occurs because the dispersion of SF-10 in the near-infrared does not follow the usual dispersion law for transparent glasses in the optical, $dn/d\lambda \propto \lambda^{-3}$. Instead of a monotonically decreasing dispersion with increasing wavelength, SF-10 has a dispersion minimum at $\sim 1.7\mu\text{m}$ (Figure 8) at room temperature. This leads to theoretical relative order separations also shown in Figure 8. Both plots compare SF-10 and ZnSe. SF-10 has a similar dispersion function at 77K as at room temperature.

3.4. Slit Viewer Optics

Complementing the spectrograph optical train is a slit viewing mode (Figure 4). Light not transmitted through the slit is reflected by the polished slit substrate into the secondary slit viewing train. This allows viewing a K_s image of the reflective slit for rapidly steering science targets into the slit. A remotely-controlled drive motor outside the Dewar turns an internal flip-mirror between the slit-viewing and spectrographic positions in ~ 10 sec. The flip mirror is located between the doublet and singlet of the spectrograph camera. The slit viewing optical prescription is listed in Table 2. Since the slit viewing mode is not intended for photometric imaging, all lenses in the slit viewing train are from manufacturer's stock to reduce material costs.

Light reflected from the slit is collimated by a CaF₂ lens and passes through a Lyot Stop sized to the pupil diameter of 5.1 mm. The collimated beam is then steered by two gold-coated fold mirrors to the spectrograph camera assembly. The beam also passes through a K_s filter mounted between the fold mirrors (tilted 5° away from the spectrograph elements to reduce light contamination). The slit viewing filter can be changed by opening the dewar. Lastly the beam is refocused onto the detector by the combined action of a CaF₂ lens and the final Infrasil lens of the spectrograph camera (Figure 4). The gold-coated flip mirror steers the light from the CaF₂ lens towards the final Infrasil lens and detector. The plate scale of the slit viewer is 0.27"/pixel, corresponding to an $f/18.85$ beam. This plate scale was chosen to give a FOV (35") large enough to aid the identification of targets in confused fields (Figure 7). The slit-viewer design gives 65% encircled energy diameters of ≤ 3 pixels on axis and ≤ 4 pixels at the edge of the FOV.

Light leakage from the slit viewing train when in spectroscopy mode is minimal because the flip mirror mechanism blocks the slit viewing beam just past the second slit viewing lens with a shaped baffle plate when not in use (Figure 2). We gave extra care to minimize this source of stray light in such close proximity to the detector.

4. MECHANICAL DESIGN & ALIGNMENT

4.1. Mechanical Design

AutoCAD Version 14.0 and Mechanical Desktop 2.0 (Autodesk, San Rafael, CA) were used for the mechanical

design. The optics were designed assuming all elements inside the Dewar are at 77K. Since the optical mounts are machined at room temperature, distances between elements required by the optical prescription are adjusted for the linear expansion of materials (Table 3) prior to the mechanical design and fabrication. Thus upon cooling the elements are correctly positioned.

All optical mounts were fabricated from the aluminum alloy 6061-T6, the same material used for the off-axis paraboloid and grating substrate. The mounts are attached to a 'T' cross-section aluminum 'optical bench' extending from the Dewar's cold plate. The use of only one material for all mounts reduced Coefficient of Thermal Expansion (CTE) effects and eased the difficulty of achieving good optical alignment at 77K. The aluminum optical bench, off-axis paraboloid, and grating substrate were thermally cycled between room temperature and 77K multiple times prior to final finishing to stabilize them.

The prism is constrained through a system of six aluminum pads that form a semi-kinematic mount (Figure 9). Three spring plungers oppose the pads in three dimensions and each exerts 1.0 – 1.6 lbs force to constrain the ~ 0.7 pound prism. Between each pad and the prism material is an Indium shim to prevent abrasion (Figure 9).

To accommodate differing thermal contractions all lenses are mounted in lens barrels with oversized inside diameters to prevent crushing. Retaining rings compress spring wave washers against the outer annulus of lens faces to accommodate differences in axial contraction during cooldowns.

The flip mirror is driven by an externally mounted 30 VDC motor. A shaft directly couples the external motor to the flip mirror through an O-ring rotary seal at the Dewar wall. The O-ring seal and a flexible coupling inside the dewar make up for small positional and axial changes upon cooling the instrument. Mirror position is controlled by a logic circuit involving a remotely operated toggle switch at the observer's station and limit switches engaged by the motor shaft outside of the Dewar. Placement of the limit switches outside the Dewar allows adjustment of the mirror-throw while the instrument is cold.

The double-shielded dewar uses only ~ 1 liter of LN₂ per night of observing.

4.2. Stray Light Reduction

All appropriate surfaces are painted black for stray light reduction. After using one primer coat of the two-part 9924 Wash Primer, black polyurethane Aeroglaze Z-306 paint (Lord Corporation, Erie, PA) mixed with carbon black powder was applied in two or more coatings to all exposed aluminum surfaces (Hunter et al. 1996).

The optical element mounts were designed to minimize stray light. Lenses are mounted within cylindrical aluminum tubes, as mentioned above. Particular attention was devoted to reducing stray light adjacent to the prism. Since the reflective slit is close to the prism, both optical paths past the slit are well enclosed in tubes. The prism itself is enclosed in a mount that exposes only the entrance and exit faces to the optical beam. Another critical area was that near the detector. To reduce stray light the final

¹¹ Grating cross-dispersers usually give an order separation $\propto \lambda^2$ (Schroeder 1987).

spectrograph camera and flip mirror assembly were placed within a rectangular enclosure that extends nearly to the cold plate to prevent the direct illumination of the detector by stray light from the shield walls (Figure 3). All transmissive elements in the spectrograph train were AR coated.

4.3. Alignment

Alignment of the optical trains was completed in two parts - internal element alignment and alignment with the telescope secondary. First, alignment within the instrument was conducted in the lab with a HeNe laser. As discussed above, because all element mounts were made from aluminum, the relative alignment of the optical elements was preserved upon cooling from room temperature to 77K. A telescope simulator was used to re-image a neon illuminated point source onto the slit plane to check focus. The slit-viewing collimating lens and spectrograph f/conversion lens positions were adjusted to make the slit-viewer field and the spectrum confocal with the slit.

Second, the independent optical paths of the spectrograph and slit viewer were co-aligned with the telescope secondary through an iterative process. Using a gimbaled sighting scope mounted on the telescope at the same position as CorMASS normally mounts, the scope was centered on the center of the secondary. The scope (with its directional alignment preserved) was transferred to a cassegrain-mounting-plate-simulator in the lab and sighted onto a paper disk the diameter of the secondary and mounted at the distance of the secondary. CorMASS was then mounted onto the simulator and a neon lamp was used to trace the *f*/cone of both optical paths at the distance of a paper disk. Initially, the spectrograph *f*/cone was found to be aligned within 0.5° of the secondary (centers within 1 inch at the slit-secondary distance of 135 inches), but the slit viewing *f*/cone was found to be displaced 4 inches. The slit viewing train elements were re-aligned and a subsequent test showed the alignment to have improved to within 0.5°.

Peak-up of both trains relative to the secondary can be fine-tuned by adjusting the position of 4 mounting blocks that attach the instrument to the Cassegrain mounting plate.

5. ELECTRONICS & DATA ACQUISITION

A set of MCE-3 electronics from Infrared Laboratories provides clocking and readout of the NICMOS 3 array. Four 16-bit analog-to-digital converters sample the output of each of the four NICMOS 3 quadrants with a pixel dwell time of 3 μ sec. A complete read of the array requires 51 msec. Data are recorded in a standard double-correlated sampling sequence: reset, read₁, integration delay (t_{int}), read₂. The reset timing is identical to the read timing with a pixel dwell time of 3 μ sec. A fiber-optic interface transmits the sampled data from the telescope to the control room where a custom interface provides for buffering of the frames into a frame-grabber card in a Pentium-based data-acquisition computer. The computer stores the raw reads as two-plane FITS images and displays the read₂ – read₁ frame difference for real-time analysis by the observer.

A custom DOS-based user interface provides a variety of control features such as background subtraction of

stored images and Ethernet connection to the Telescope Control System (TCS). There are two acquisition modes: continuous-acquisition and single frame modes. The former provides a real-time stream of typically short integration frames (≥ 0.5 sec) useful for steering objects into the slit.

6. PERFORMANCE

Detector and instrument performance are summarized in Table 4. Average spectrograph throughput is ≈ 0.05 , $J = 0.07$, $H = 0.13$, and $K = 0.10$. Figure 10 gives throughput as a function of wavelength and order, and includes transmission losses from the atmosphere, telescope, instrument and detector. The spectrograph sensitivity is $J = 14.6$, $H = 14.9$, and $K = 14.0$ in $t_{int} = 3600$ sec for $S/N = 5$. The spectrograph performance was determined by analyzing the reduced spectrum of the Faint HST standard P565-C (Persson et al. 1998) observed in clear conditions and with seeing $\lesssim 2''$ at K . This sensitivity conforms to experience; in clear conditions we normally observe $K_s \sim 13$ objects for $t_{int} \sim 3000$ sec, and $K_s \sim 14$ objects for $t_{int} \sim 4000$ sec, to ensure sufficient S/N.

Also plotted in Figure 10 are normalized dome flat response curves for each order. The response curves displayed are the normalized spectra (raw DN) from the sum of 45 *flat lamp on – lamp off* differenced pairs accumulated over 9 nights in May 2000.

The Slit Viewer sensitivity is $K_s \sim 13$ in 2 sec for a $\sigma = 5$ point source detection with a subtracted background under good seeing conditions. In practice $t_{int} \sim 2-5$ sec continuous acquisition frames without background subtraction are used to detect and steer $K_s \leq 13$ sources into the slit. For $K_s = 14$ (the faintest sources practical to observe spectroscopically with CorMASS) $t_{int} \sim 20$ sec frames are used. Subtraction of a previously saved sky background integration is often used to aid detection of fainter sources. Slit Viewer throughput at K_s is ~ 0.20 e^- out of the array per photon in at the top of the atmosphere. This throughput includes transmission losses from the atmosphere, telescope, instrument optics, and detector QE. The slit viewer performance was determined by analyzing images of P-565C in the same conditions mentioned above.

Persistence is observed in the CorMASS detector when very bright objects, e.g. $V < 6$ calibration stars, are observed spectroscopically. $V \geq 8$ calibrators are preferred for this reason.

7. DATA REDUCTION & SPECTRA

7.1. Data Reduction

CorMASS first light observations occurred during 1999 August 22-25, with seven additional runs through 2000 August.

Single frame integration times of 100-300 seconds are typically taken with telescope nods of $\sim 4.5 - 7''$ along the slit between each integration. Frame integration times are reduced when airglow and/or atmospheric water content are judged to be highly variable to maintain effective sky subtraction.

Dome flats are taken before the start of each night's observing. Dome illumination for the flats is provided by a

10W QTH (Quartz, Tungsten and Halogen) lamp mounted above the telescope secondary.

Spectral observations of calibrator stars for atmospheric correction are taken at airmasses within ± 0.1 airmass of the target observations. A-stars from the Elias standards (Elias et al. 1982) and bright late-F and G-stars have been used as calibrators.

Following bad-pixel correction, the flat field and flux calibration spectral images are corrected for NICMOS 3 *shading*. This is a noiseless exponential change in pixel bias based upon position, time since last pixel read, and detector temperature. The changing temperature of the detector readout amplifiers during readout causes an exponentially varying bias in the direction orthogonal to the pixel clocking, or along the columns (Böker et al. 2000). The columns are \sim perpendicular to the orders (Figure 7). To remove this artifact a quadratic is fit to a row-by-row clipped median of the top quarter of the array, the portion unused by the spectrograph. The fit is extrapolated to 128 rows for the top two quadrants, duplicated for the bottom two quadrants, and subtracted row-by-row from all pixels. The quadratic fit agrees well with row medians of 'quasi-dark' images taken with the flip mirror half-way between spectrograph and slit-viewing mode.

Spectra are reduced using standard routines in IRAF¹². Images are flat fielded using a pixel responsivity solution derived from the APFLATTEN task using dome flats from all nights of the run summed together. Nodded image pairs for science objects are subtracted against each other to remove sky background to first-order and shading effects. The shading correction discussed above is not applied to science object images because the subtraction of adjacent nodded images removes the effect to a comparable noise level as the quadratic fit method.

The APALL task is then used for spectral extraction. Wavelength calibration is accomplished by using line identifications from spectral observations of planetary nebulae, e.g. NGC 7027 and NGC 6210. A third-order polynomial is fit to the identified lines to derive a dispersion solution across the orders. The fit residual RMS is $\leq \frac{1}{5}$ pixel (2.25 \AA) across the wavelength coverage. The use of OH airglow lines was rejected because at the resolution of CorMASS ($R \sim 300$), many airglow lines are blended together, especially in the H-band, making line identifications problematic.

Telluric absorption effects are removed by dividing by the reduced spectrum of a standard observed at similar airmass and hand corrected for stellar H Paschen and Brackett recombination lines as required. The ratio is then multiplied by a black-body with a temperature equal to the effective temperature of the stellar type of the calibrator observed (Tokunaga 2000). Lastly, all observations for each order are weighted by the spectra mean and combined with the SCOMBINE task using a trimmed average. Orders are stitched together with SCOMBINE after hand deletion of noisy data at the ends of the orders.

7.2. Spectra

A spectrum of the infrared bright planetary nebula NGC 7027 is shown in Figure 11. The plentiful emission lines of

planetary nebulae, primarily H and He lines, are used for wavelength calibration. CorMASS' wavelength coverage and efficiency are well suited for the study of numerous types of objects including quasars, novae, and emission line objects.

Spectra of the low-mass objects VB 10 (M 8V), 2MASSW J1507476-162738 (L 5V, hereafter 2M1507), and the T-dwarf 2MASSI J0559191-140448 (hereafter 2M0559) are presented in Figure 12. A full spectral sequence and NIR L-dwarf features will be discussed in another paper (Wilson et al. 2000).

CorMASS spectroscopically confirmed the classification of 2M0559 ($J = 13.83 \pm 0.03$) during the instrument's second run (Burgasser et al. 2000). 2M0559 is 0.4 mag brighter than Gl 229B and more than 1 mag brighter than the other field T-dwarfs discovered to date. This object's brightness will aid broad wavelength and high resolution study of its spectral class.

While no methane combination and overtone absorption features at 1.6 and 2.2 μm (the features that define the T-dwarf class) are evident in 2M1507, weak fundamental methane absorption has been discovered at 3.3 μm in 2M1507 and in an L 7.5 (Noll et al. 2000). This suggests that the transition from CO to CH₄ as the primary carbon-bearing molecule as effective temperatures decrease commences as early as L 5V.

8. CONCLUSION

This paper described the newly built and commissioned NIR low-resolution ($R \sim 300$) prism cross-dispersed spectrograph CorMASS in operation on the Palomar 60-inch telescope. This instrument was designed primarily for the identification of late-M and L-dwarf spectral features. CorMASS spectra of low-mass objects from the L, M, and T-dwarf classes, as well as the planetary nebula NGC 7027, were presented. Instrument characteristics include:

1. Low-cost compact design.
2. Simultaneous λ coverage of the $zJHK$ NIR bands with $R \sim 300$.
3. A two-position flip mirror for imaging an alternate slit viewing train.
4. Spectrograph sensitivity of $K = 14.0$ in $t_{int} = 3600$ sec for S/N=5.

We wish to thank the Cornell University LASSP (Laboratory of Applied and Solid-State Physics) Machine Shop and the UMASS Physics Machine Shop for their professional and timely machining. Many thanks to Hal Petrie for providing drawings and important information about the 60-inch along the way. We also wish to acknowledge Bob Thicksten and the rest of the Palomar Observatory Staff for their wonderful attitudes and invaluable assistance with the interface of CorMASS to the telescope and professional telescope operations. Special thanks to Night Assistants Skip Staples and Karl Dunscombe for their expertise and support as we learned how to observe with this new instrument. It is truly an enjoyable experience observing on Palomar Mountain. We also wish to thank Eric

¹² IRAF is distributed by the National Optical Astronomy Observatories, which are operated by the Association of Universities for Research in Astronomy, Inc., under cooperative agreement with the National Science Foundation.

Persson and David Murphy for information on the Palomar 60-inch prescription and instrument mounting constraints. We largely duplicated the mounting scheme of their P60 IR camera. Thanks to Tom Murphy for making available his list of late-F and G-star calibration standards. We benefited from useful discussions with Scott Milligan of Telic Optics on optical design and element properties, as well as the thorough final report for the 2MASS Prototype Camera redesign produced by his company. We greatly benefited from Bernhard Brandl's advice and experience with optical and mechanical design, as well

as his careful reading of a draft of this paper. We also wish to acknowledge the influence of Jeff Van Cleve and the SCORE (SIRTF Cornell Echelle Spectrograph) philosophy of a cross-dispersed echelle with minimal moving parts. JCW and JDS acknowledge support by NASA grant NAG5-4376. This publication makes use of data from the Two Micron All Sky Survey, which is a joint project of the University of Massachusetts and the Infrared Processing and Analysis Center, funded by the National Aeronautics and Space Administration and the National Science Foundation.

REFERENCES

Böker, T., et al., 2000, NICMOS Instrument Handbook, Version 4.0, (Baltimore:STScI)

Bowen, I. S. & Rule, B. H., 1966, S&T, 32, 184

Burgasser, A. J., Wilson, J. C., Kirkpatrick, J. D., Skrutskie, M. F., Colombo, M. R., Enos, A. T., Smith, J. D., Henderson, C. P., Gizis, J. E., Brown, M. E., & Houck, J. R., 2000, AJ, 120, 1100

Burrows, A. & Sharp, C. M., 1999, ApJ, 512, 843

Casement, L. S., McLean, I. S., & Fischer, R. E., 1993, Proc. SPIE, 1946, 569

Elias, J. H., Frogel, J. A., Matthews, K., & Neugebauer, G., 1982, AJ, 87, 1029

Epcstein, N., 1997, in The Impact of Large-Scale Near-IR Sky Surveys, ed. F. Garzon (Dordrecht: Kluwer), 15

Fegley, B., Jr. & Lodders, K., 1996, ApJ, 472, 37

Fukugita, M., Ichikawa, T., Gunn, J. E., Doi, M., Shimasaku, K., & Schneider, D. P., 1996, AJ, 111, 1748

Gunn, J. E. & Weinberg, D. H., 1995, in Wide Field Spectroscopy and the Distant Universe, ed. S. Maddox & A. Aragón-Salamanca (Singapore: World Scientific), 3

Hunter, T. R., Benford, D. J., & Serabyn, E., 1996, PASP, 108, 1042

Kirkpatrick, J. D., Reid, I. N., Liebert, J., Cutri, B. M., Nelson, B., Beichman, C. A., Dahn, C. C., Monet, D. G., Gizis, J. E., & Skrutskie, M. F., 1999, ApJ, 519, 802

Kirkpatrick, J. D., Reid, I. N., Liebert, J., Gizis, J. E., Burgasser, A. J., Monet, D. G., Dahn, C. C., & Nelson, B., 2000a, AJ, 120, 447

Kirkpatrick, J. D., 2000b, AAS 196th Meeting, Session 20.02

Leggett, S. K., 1992, ApJS, 82, 351

Loewen, E. G., Nevière, M., & Maystre, D., 1977, Applied Optics, 16, 2711

Martin, E. L., Basri, G., Delfosse, X., & Forveille, T., 1997, A&A, 327, L29

Nakajima, T., Oppenheimer, B. R., Kulkarni, S. R., Golimowski, D. A., Matthews, K., & Durrance, S. T., 1995, Nature, 378, 463

Noll, K. S., Geballe, T. R., Leggett, S. K., & Marley, M. S., 2000, ApJ, accepted

Oliva, E. & Gennari, S., 1997, A&A, 128, 599

Oppenheimer, B. R., Kulkarni, S. R., Matthews, K., & van Kerkwijk, M. H., 1998, ApJ, 502, 932

Murphy, D. C., Persson, S. E., Pahre, M. A., Sivaramakrishnan, A., & Djorgovski, S. G., 1995, PASP, 107, 1234

Persson, S. E., Murphy, D. C., Krzeminski, W., Roth, M., & Rieke, M. J., 1998, AJ, 116, 2475

Reid, I. N., Kirkpatrick, J. D., Liebert, J., Burrows, A., Gizis, J. E., Burgasser, A., Dahn, C. C., Monet, D., Cutri, R., Beichman, C. A., & Skrutskie, M., 1999, ApJ, 521, 613

Schroeder, D. J., 1987, Astronomical Optics (San Diego: Academic Press)

Skrutskie, M. F., et al. 1997, in The Impact of Large-Scale Near-IR Sky Surveys, ed. F. Garzon (Dordrecht: Kluwer), 25

Tokunaga, A. T., 2000, in Allen's Astrophysical Quantities, Fourth Edition, ed. A. N. Cox (New York: Springer-Verlag)

Touloukian, Y. S., ed., 1975, Thermal Properties of Matter (New York: IFI/Plenum)

Wilson, J. C., Skrutskie, M. F., Gizis, J. E., Monet, D., Kirkpatrick, J. D., & Houck, J. R., 2000, ApJ, in preparation



FIG. 1.—CorMASS mounted at the Cassegrain Focus of the Palomar 60-inch telescope. On the right side of the Dewar is the externally mounted flip-mirror drive assembly. In the foreground to the left is the box containing the Infrared Labs MCE-3 electronics for clocking and array readout. The telescope visual guide camera is to the right of the Dewar mounted at 45° .

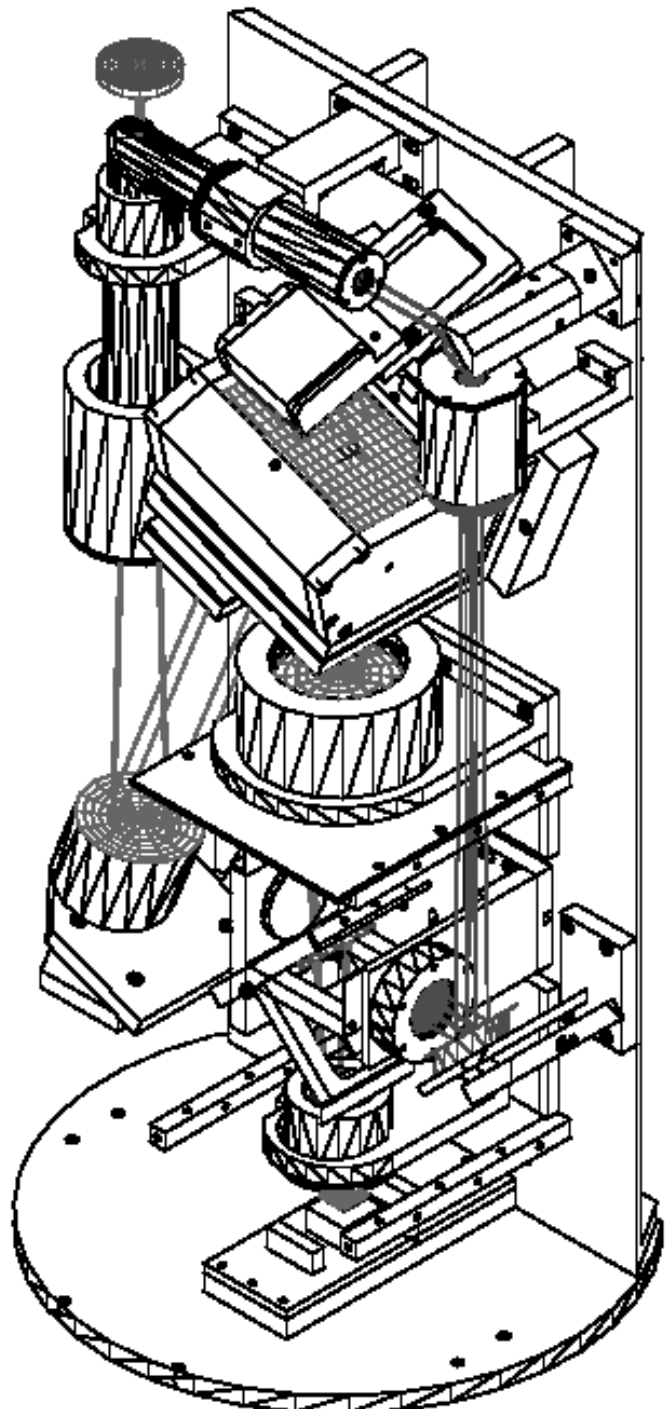


FIG. 2.— The optical bench schematic. The long dimension is 14.5''. This bench is easily removed from the Dewar for lab testing and alignment. The flip-mirror is shown in both spectrograph and slit viewing positions. The sides of the spectrograph camera enclosure have been removed from this drawing for display purposes.

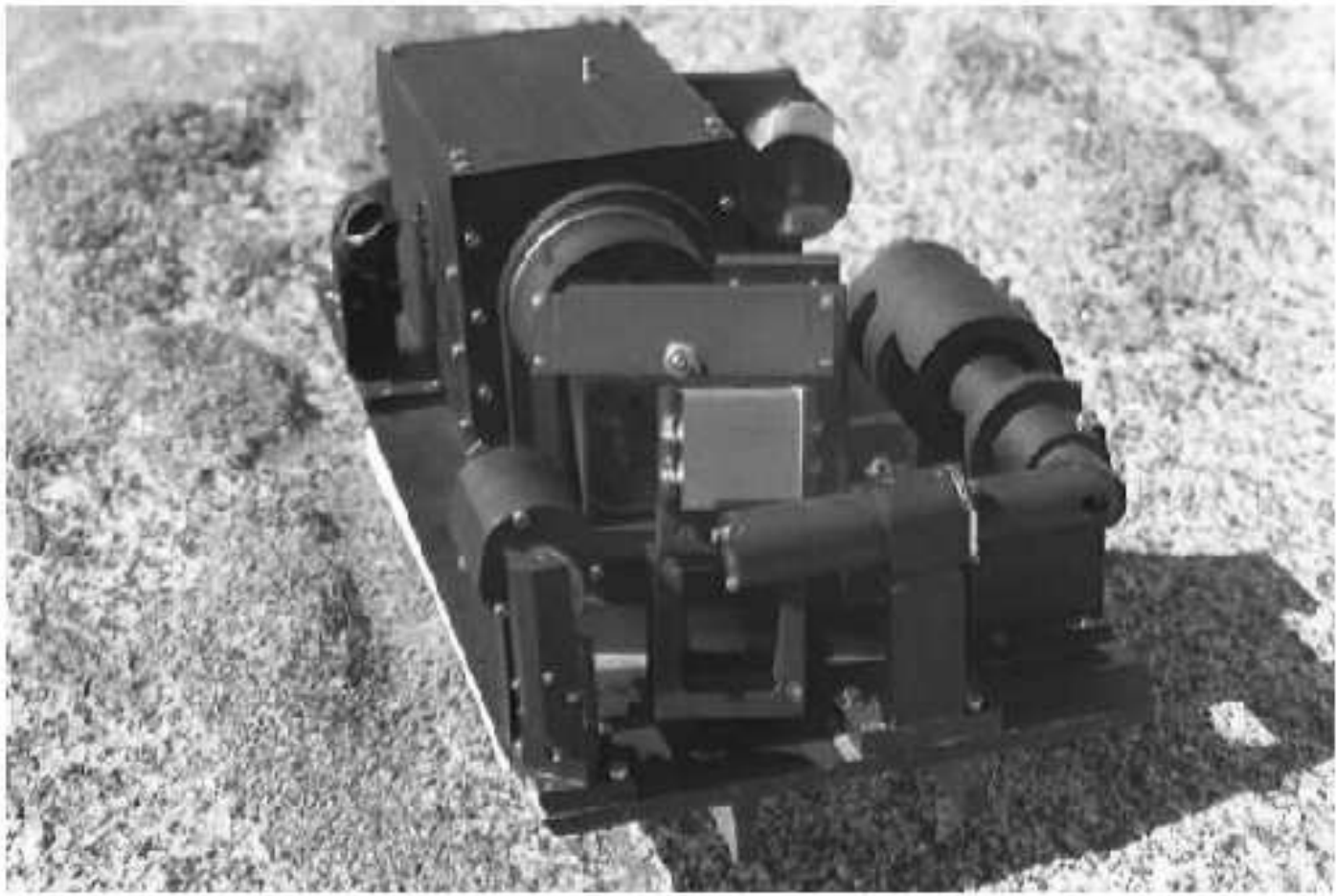


FIG. 3.— The optical bench removed from the Dewar. Optical Element mount tubes surrounding the prism are seen in the foreground and the spectrograph camera and flip-mirror assembly is at the far end.

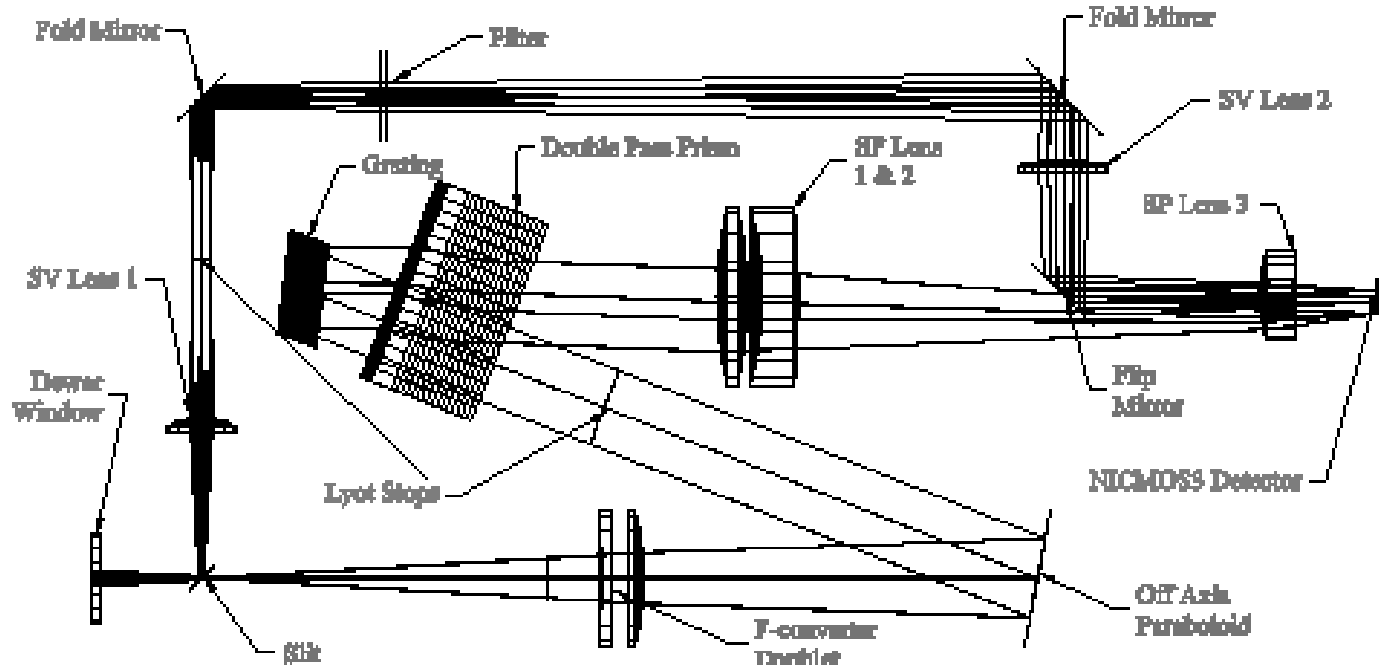


FIG. 4.— Optical paths for the spectrograph and slit viewer. The paths split at the slit plane. The externally driven two-position flip mirror selects either path for imaging onto the detector.

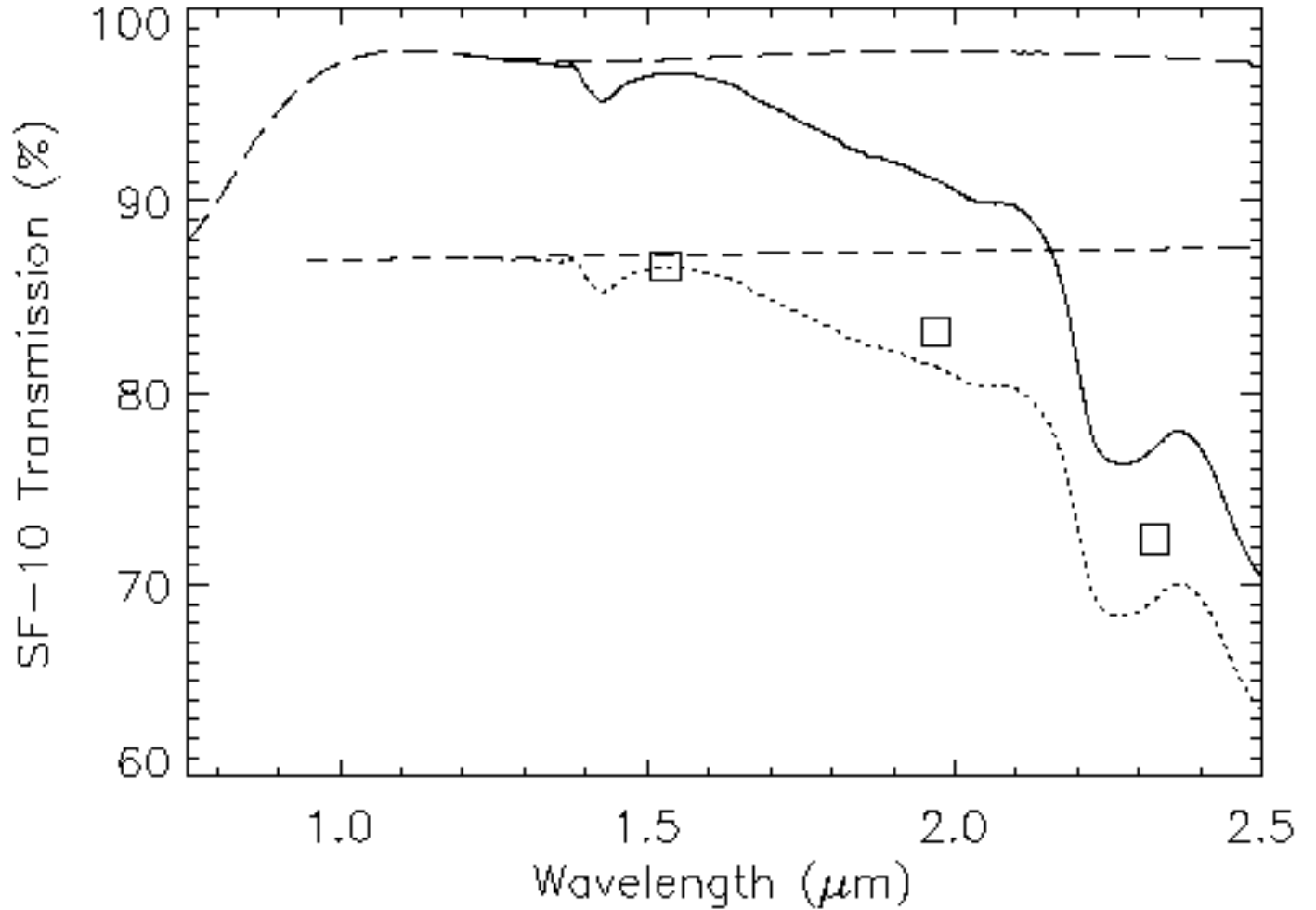


FIG. 5.— Measured internal transmission of SF-10 (21.7 mm thickness) (dotted line) including theoretical reflection losses from two air-glass interfaces (dashed line). Square boxes represent absorption prediction derived from Schott Data Sheet for uncoated material. Expected AR coating performance for two air-glass interfaces (long dashed line) is applied to the measured internal transmission to estimate total transmission for one prism pass in CorMASS (solid line).

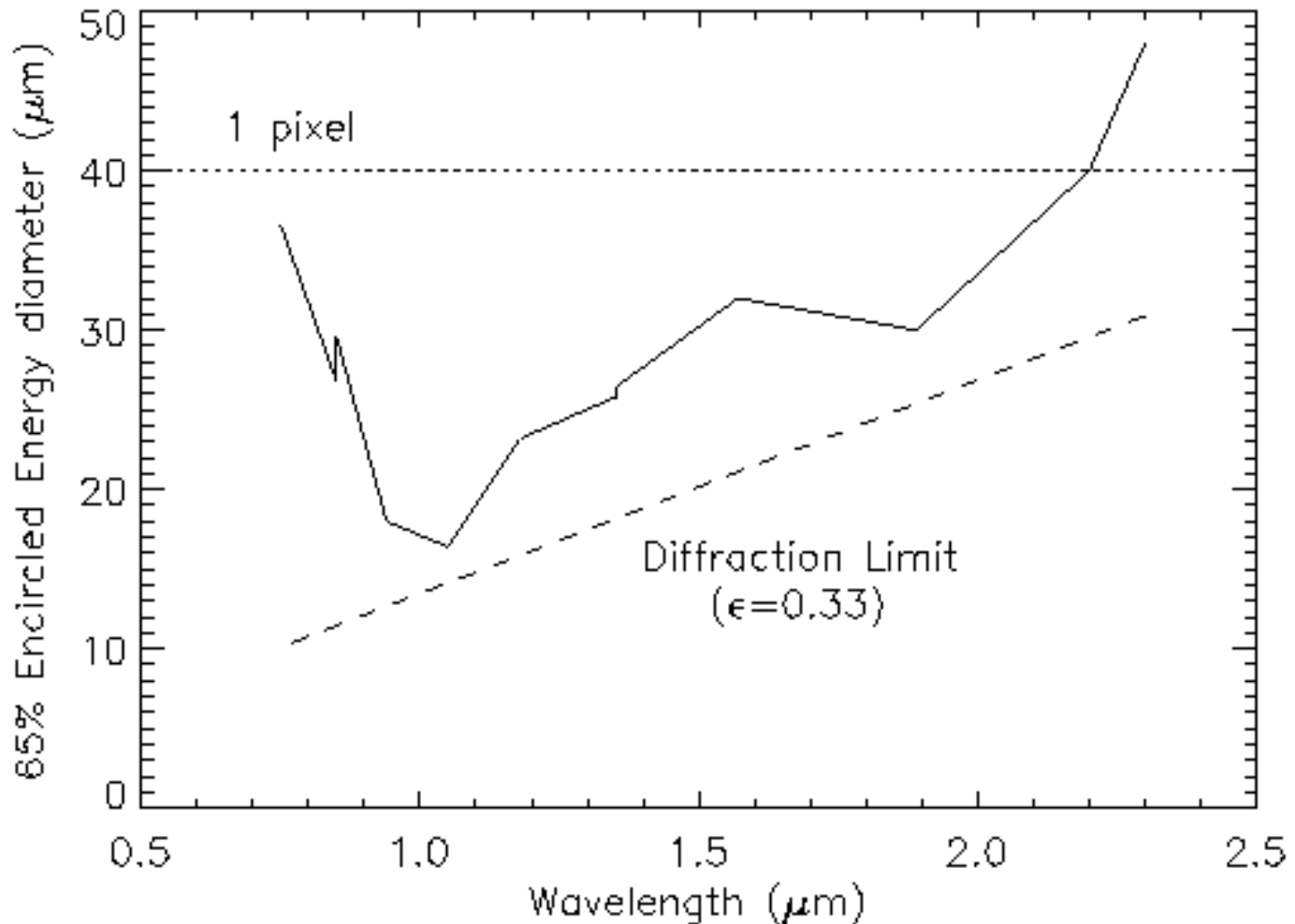


FIG. 6.— The 65% Encircled Energy diameter v. wavelength for the spectrograph (entire slit FOV). The approximate diffraction limit, dashed line, and the pixel size, dotted line, are also shown.

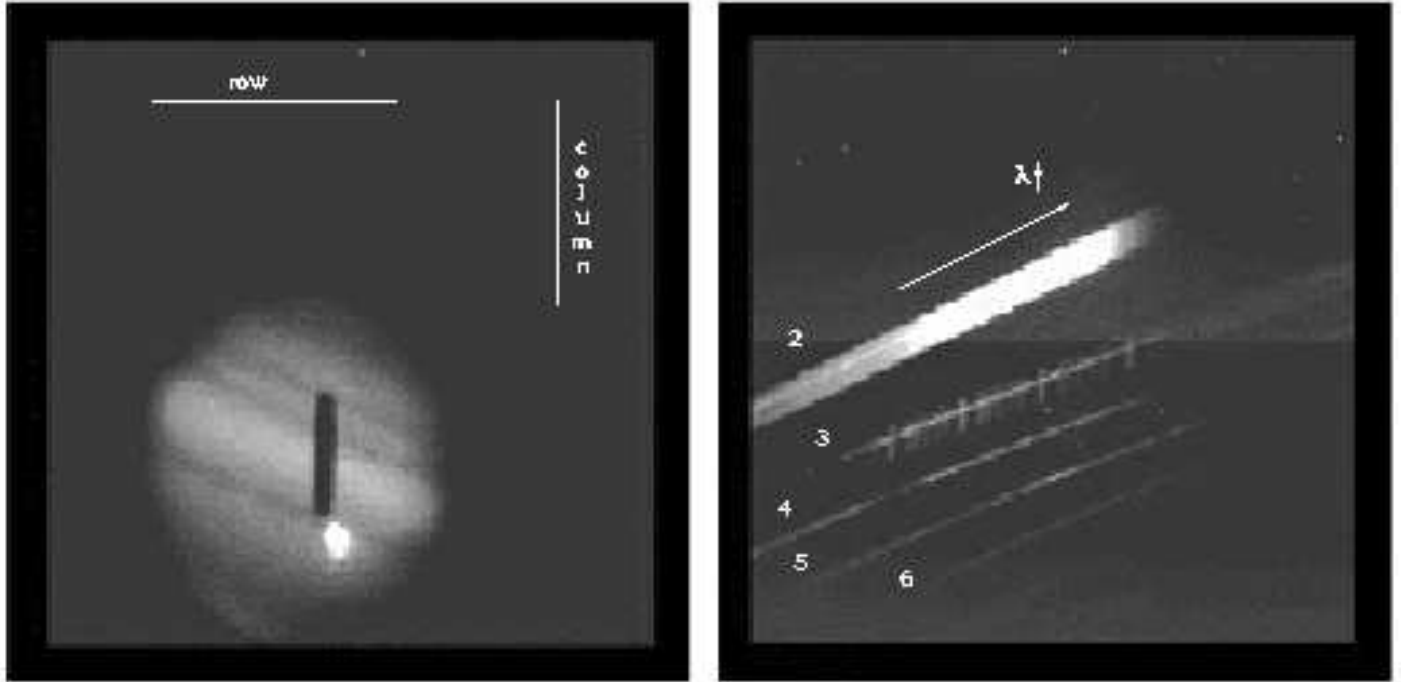


FIG. 7.— Slit Viewer and Spectrograph images. (a) Jupiter fills the 35'' Slit Viewer FOV, with Io just below the $2'' \times 15''$ slit. Row and column directions are indicated. (b) The spectral image displays a Wolf-Rayet near the middle of the slit. The second order is at the top, sixth order at the bottom. The thermal emission of the atmosphere increases rapidly in the second order then abruptly cuts off at $\sim 2.5\mu\text{m}$. Sky lines dominate the third order (H-band). NICMOS3 shading anomaly is seen at the bottom of the quadrants prior to correction. Order numbers and direction of increasing wavelength are indicated.

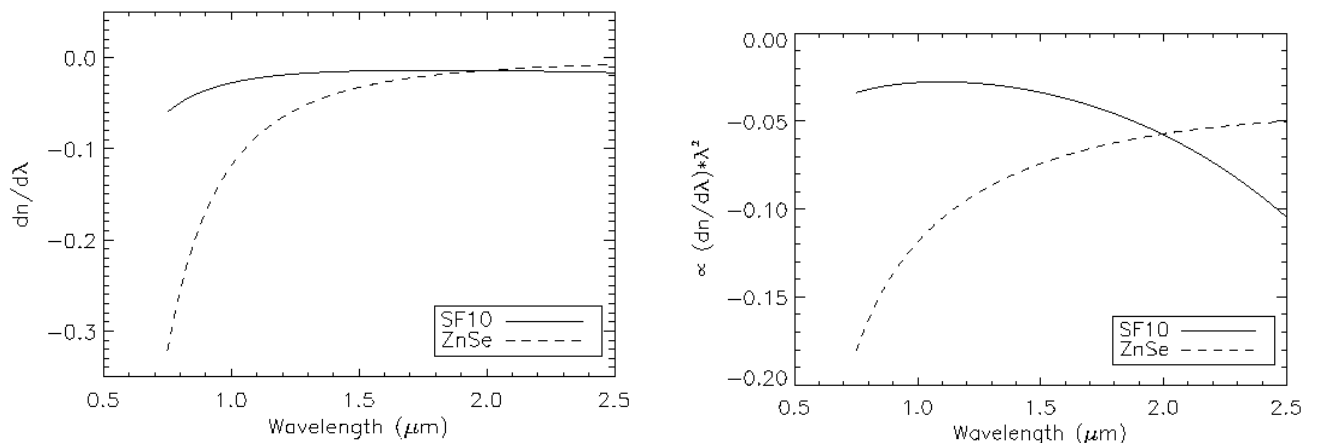


FIG. 8.— (a) Dispersion $(dn/d\lambda)$ vs. λ and (b) Relative order separation vs. λ for Schott dense flint SF-10 and ZnSe at room temperature. SF-10 is used for the cross-dispersing double pass prism.

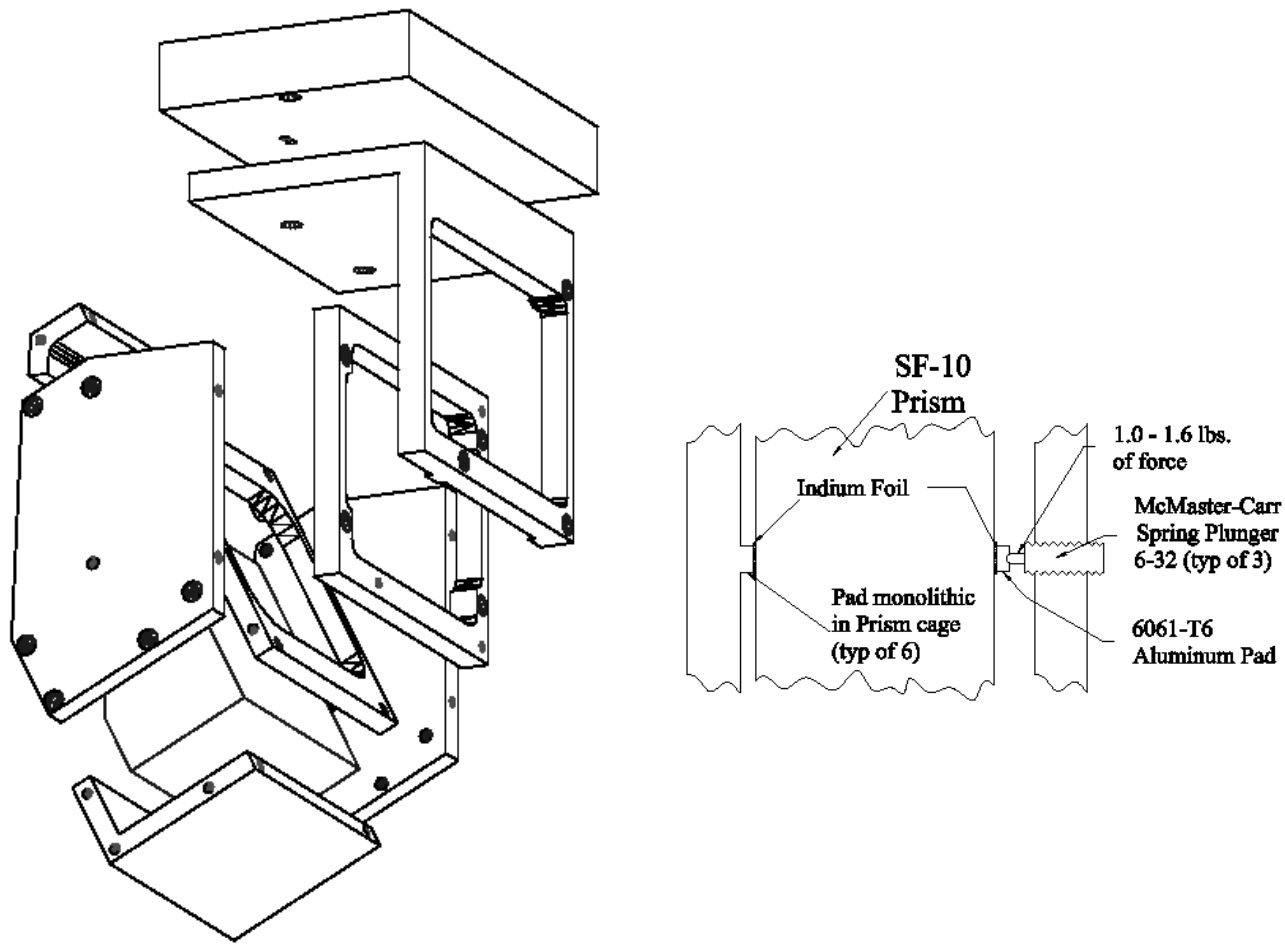


FIG. 9.— (a) The prism cage constrains the prism in a semi-kinematic mount and provides stray-light control. (b) The prism holding scheme includes three spring plungers that oppose six monolithic pads in 3-dimensions to secure the prism and compensate for thermal expansion effects.

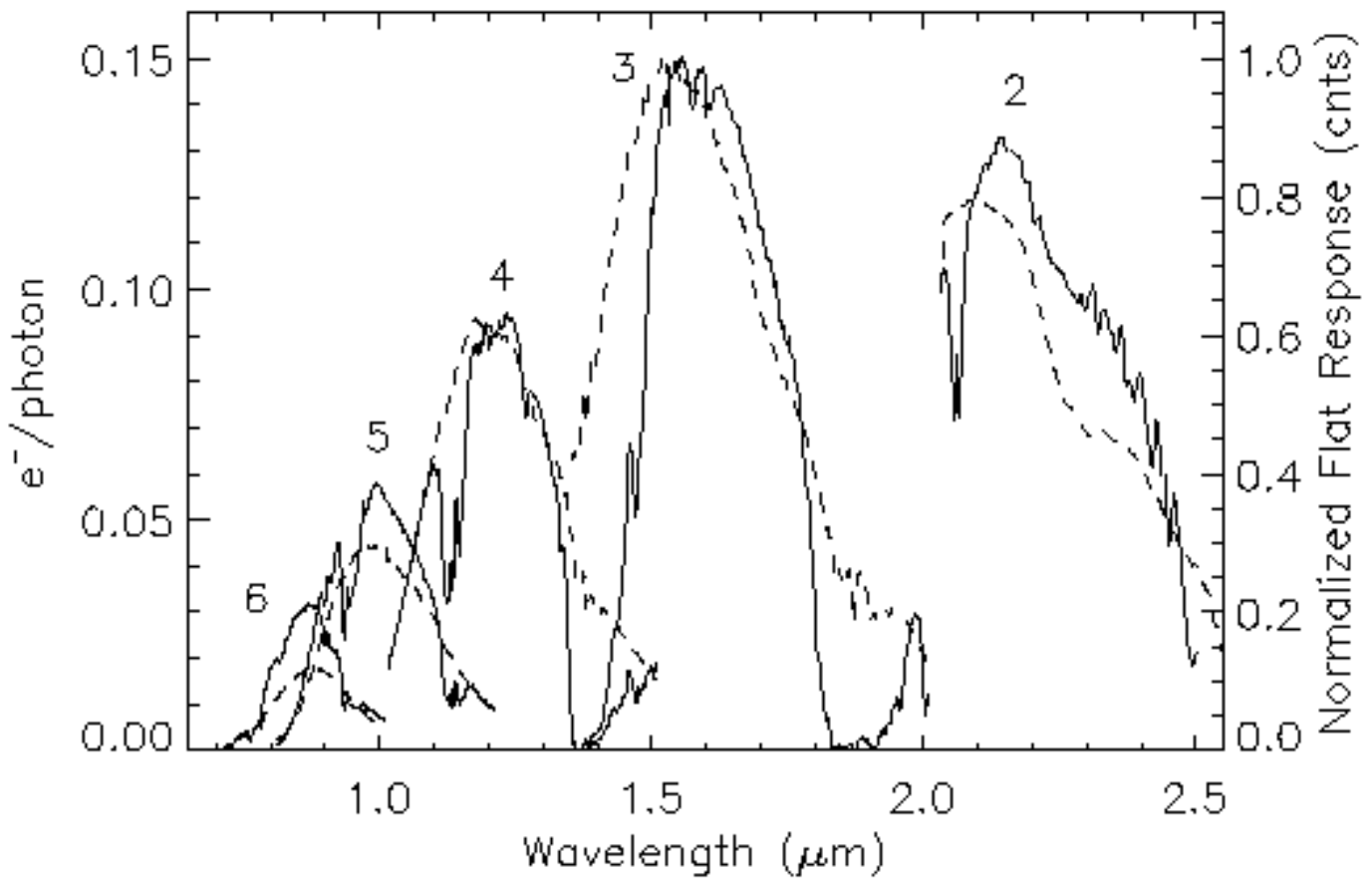


FIG. 10.— Spectrograph throughput v. wavelength for each order (solid line). Order number is identified at the top of each throughput curve. Throughput is in electrons out of the detector per photons in at the top of the atmosphere. Also plotted for comparison is the dome flat response in raw counts normalized to the peak in H (dashed line).

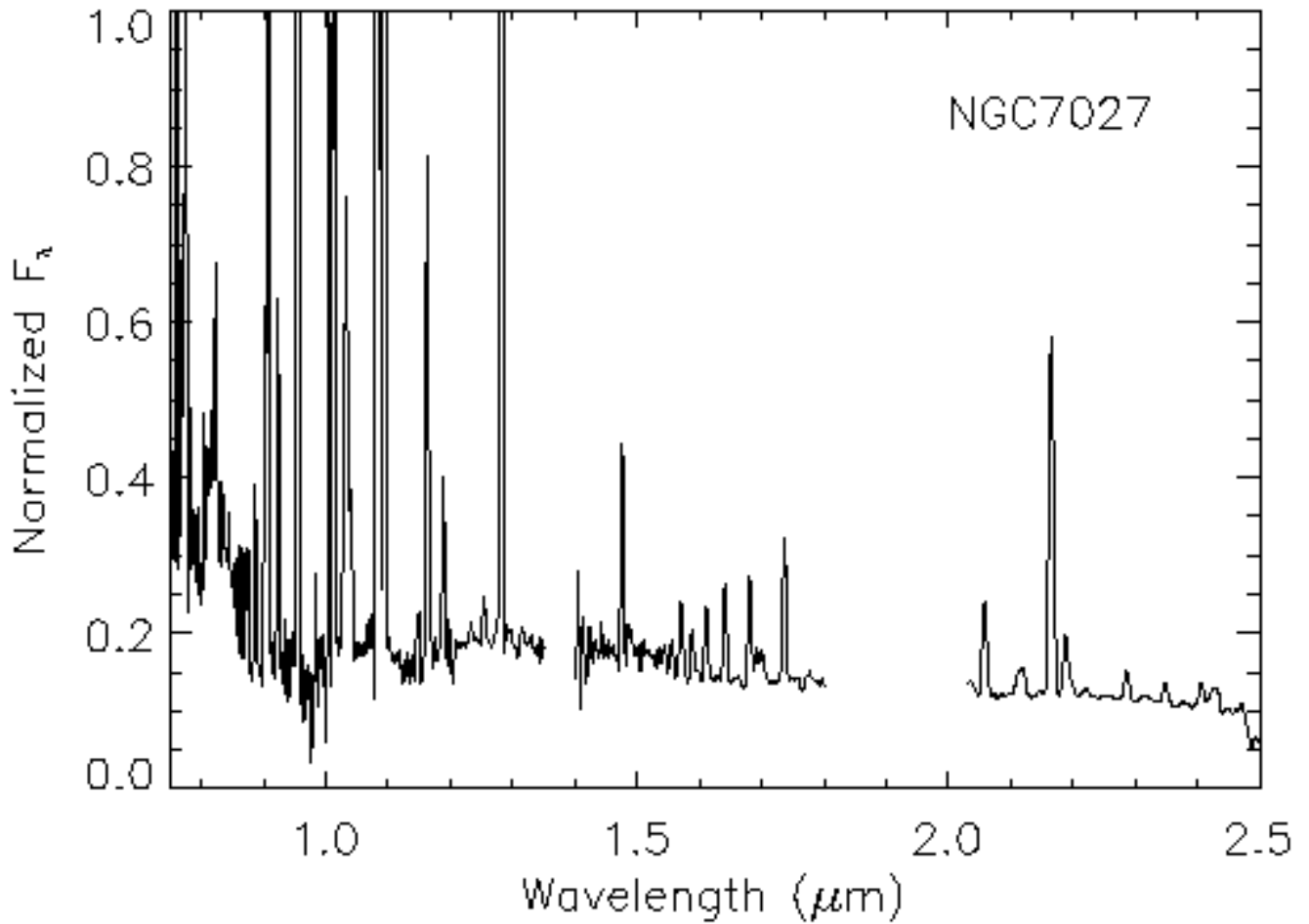


FIG. 11.—CorMASS spectra of NGC 7027. This well studied planetary nebula was observed 24 October 99 for $t_{\text{int}} = 20$ sec. 38 distinct emission lines across 6 orders were identified for use within IRAF to derive a dispersion solution for the wavelength calibration of program objects. This plot has been clipped to enhance fainter lines.

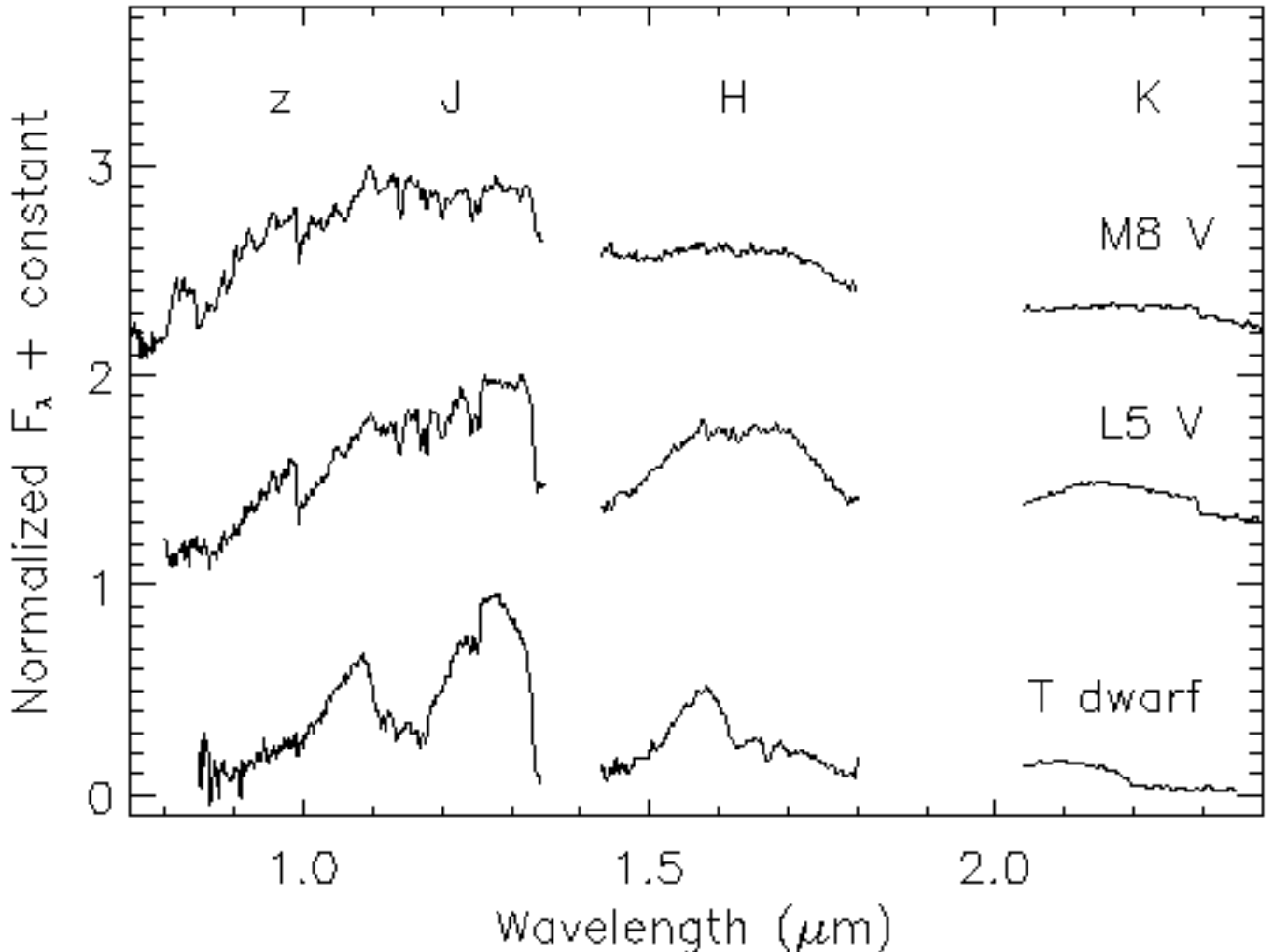


FIG. 12.— CorMASS $zJHK$ spectra of three low-mass objects: M 8V (VB 10), L 5V (2MASSW J1507476-162738, hereafter J1507), and a T-dwarf (2MASSI J0559191-140448, hereafter J0559). VB 10 ($K = 8.80$, Leggett (1992)), was observed 22 August 99 for $t_{\text{int}} = 1080$ sec. J1507 ($K_s = 11.30$, Kirkpatrick et al. (2000a)), was observed 20 April 00 for $t_{\text{int}} = 1800$ sec. J0559 ($K_s = 13.61$, Burgasser et al. (2000)), was observed 24 October 99 for $t_{\text{int}} = 2400$ sec. Data between bands was not usable due to poor atmospheric subtraction.

TABLE 1
PALOMAR 60-INCH AND SPECTROGRAPH PRESCRIPTION

Surface	Radius ^a (mm)	Thickness ^{a,b} (mm)	Material	Diameter (mm)
Central Obscuration	...	~ 2900	...	640.08
Tel Primary ^c	-7619.977	-2827.918	coated Alum	1549.40
Tel Secondary ^d	-2750.003	3402.212	coated Alum	454.56
Cass Mtg Surf	...	3.917
Dewar Window (R1)	Inf	3.074	AR coated CaF ₂	25.40
Dewar Window (R2)	Inf	28.444	...	25.40
Reflective Slit ^e	Inf	114.277	SS 304	9.53
f/Converter Lens 1 (R1)	-166.870	3.000	AR coated Infrasil 301	38.10
f/Converter Lens 1 (R2)	Inf	4.189	...	38.10
f/Converter Lens 2 (R1)	Inf	4.502	AR coated CaF ₂	38.10
f/Converter Lens 2 (R2)	-79.810	101.600	...	38.10
Off-Axis Paraboloid ^f	-60.960	-143.479	Au coated Alum	38.10
Lyot Stop	...	-46.521	...	22.56
Prism 1st Pass (R1) ^g	Inf	-20.000	SF-10	...
Prism 1st Pass (R2)	Inf	-30.000
Grating ^h	Inf	30.000	Au coated Alum	...
Prism 2nd Pass (R2)	Inf	20.000	SF-10	...
Prism 2nd Pass (R1)	Inf	75.000
Camera Lens 1 (R1)	109.520	8.647	AR coated BaF ₂	50.80
Camera Lens 1 (R2)	-120.289	4.460	...	50.80
Camera Lens 2 (R1)	-94.600	10.000	AR coated Infrasil 301	50.80
Camera Lens 2 (R2)	-287.900	131.430	...	50.80
Camera Lens 3 (R1) ⁱ	36.540	10.000	AR coated Infrasil 301	50.80
Camera Lens 3 (R2)	258.750	23.569	...	50.80
Detector	NICMOS 3	10.24 ²

^aCold Dimensions (77K) for slit and below

^bDistance to next face or element

^cConic Constant: $k = -1$; Sag (mm): $(-6.5617e - 5)y^2 + (1.835e - 14)y^4$

^dConic Constant: $k = -1$; Sag (mm): $(-1.81818e - 4)y^2 + (1.743e - 11)y^4$

^eSlit rotated 45 deg to optical axis along slit axis

^fFocal Length (cold) = 12'', Decenter (cold) = 115.57mm, Off-Axis Diameter (OAD) (cold) = 3.8''

^g30 deg Prism apex angle, used in minimum deviation

^h40lines/mm, $\lambda_{blaze} = 4.8\mu\text{m}$, Blaze Angle = 5.5 deg, Richardson Grating Lab replica

ⁱCamera Lens 3 is shared with the Slit Viewing path

TABLE 2
SLIT VIEWER PRESCRIPTION

Surface	Radius ^a (mm)	Thickness ^{a,b} (mm)	Material	Diameter (mm)
Reflective Slit ^c	Inf	-41.287	SS 304	9.53
Slit Vwr Lens 1 (R1)	Inf	-4.558	CaF ₂	19.05
Slit Vwr Lens 1 (R2)	19.018	-45.146	...	19.05
Lyot Stop	Inf	-46.126	...	5.111
Fold Mirror 1	Inf	50.8	Au coated BK7	19.05
K_s Filter (R1) ^d	Inf	2.0	...	25.4
K_s Filter (R2)	Inf	193.146	...	25.4
Fold Mirror 2	Inf	-18.170	Au coated Pyrex	31.42
Slit Vwr Lens 2 (R1)	-59.819	-3.390	CaF ₂	25.4
Slit Vwr Lens 2 (R2)	Inf	-35.118	...	25.4
Flip Mirror	Inf	55.494	Au coated Pyrex	25.4
Camera Lens 3 (R1) ^e	36.540	10.000	AR coated Infrasil 301	50.80
Camera Lens 3 (R2)	258.750	23.569	...	50.80
Detector	NICMOS 3	10.24 ²

^aCold Dimensions (77K) for slit and below

^bDistance to next face or element

^cSlit rotated 45 deg to optical axis along slit axis

^dFilter tilted 5 deg towards side of Dewar for stray light control

^eCamera Lens 3 is shared with the Spectrograph path

TABLE 3
COEFFICIENTS OF THERMAL EXPANSION

Material	$\Delta L/L(\%)^a$	Reference
Alum	0.392	Casement et al. (1993) & Toulioukian (1975)
CaF ₂	0.303	Casement et al. (1993) & Toulioukian (1975)
BaF ₂	0.319	Casement et al. (1993) & Toulioukian (1975)
Infrasil-301	0.0	Type I SiO ₂ (Fused), Toulioukian (1975)
SF-10	0.127	Assume $(\Delta L/L)_{SF-10} \sim (\Delta L/L)_{Al} * \alpha(0^\circ C)_{SF-10} / \alpha(0^\circ C)_{Al}$

^a293K-77K

TABLE 4
CORMASS PERFORMANCE

Parameter	Value
Detector	NICMOS 3
Bias	0.91 V
Gain	8.5 e ⁻ /DN
Read Noise	42.5 e ⁻
Well Depth	$\sim 3.8 \times 10^5$ e ⁻
Bad Pixels	< 1%
Spec Sensitivity ^{a,b}	$J = 14.6, H = 14.9, K = 14.0$
Spec Ave Throughput ^{b,c}	$z = 0.05, J = 0.07, H = 0.13, K = 0.10$
Slit Viewer Sensitivity ^b	$K_s = 13$ in 2 sec for $\sigma = 5$
Slit Viewer Throughput ^c	0.20

^aS/N=5, $t_{int} = 3600$ sec

^bFor a point source detection with a subtracted background in clear conditions with seeing $\lesssim 2.0''$ at K.

^ce⁻/photon, includes transmission losses from the atmosphere, telescope, instrument and detector QE.